ACS APPLIED MATERIALS & INTERFACES

www.acsami.org

Research Article

Bistriazoles with a Biphenyl Core Derivative as an Electron-Favorable Bipolar Host of Efficient Blue Phosphorescent Organic Light-Emitting Diodes

Jiun-Haw Lee, Chia-Hsun Chen, Bo-Yen Lin, Yi-Hsin Lan, Yi-Mei Huang, Nai-Jing Chen, Jau-Jiun Huang, Dmytro Volyniuk, Rasa Keruckiene, Juozas Vidas Grazulevicius, Yuh-Renn Wu, Man-kit Leung,* and Tien-Lung Chiu*

Cite This: *ACS Appl. Mater. Interfaces* 2020, 12, 49895−49904

Read Online

ACCESS | Metrics & More | Article Recommendations | Supporting Information

ABSTRACT: High-quality host materials are indispensable for the construction in the emitting layer of efficient organic light-emitting diodes (OLEDs), especially in a guest and host system. The good carrier transport and energy transfer between the host and emitters are out of necessity. In this work, a wide bandgap and bipolar organic compound, 2,2′-bis(4,5-diphenyl-(1,2,4)-triazol-3-yl)-biphenyl (**BTBP**), conjugating two electron-transporting triazole moieties on a hole-transporting biphenyl core, was synthesized and characterized. The wide bandgap of 4.0 eV makes the promise in efficient energy transfer between the host and various color emitters to apply as the universal host, especially for blue emitters. The close electron and hole mobilities perform the same order of 10^{-5} $cm^2 \cdot V^{-1} \cdot s^{-1}$, identified as bipolar behavior and benefited for carrier balance at low bias. Although carrier transportation belongs to bipolar behavior at a low electrical field, the electron mobility is much faster than the hole one at a high electrical field and belongs to electron-transporting behavior. Employing the **BTBP** as the host matrix mixed with a phosphor dopant, iridium(III)bis[4,6-di-fluorophenyl-pyridinato-N,C^2]picolinate, a high-efficiency sky-blue phosphorescent organic light-emitting diode (OLED) was achieved with a maximum current efficiency of 65.9 cd/A, maximum power efficiency of 62.8 lm/W, and maximum external quantum efficiency of 30.2%.

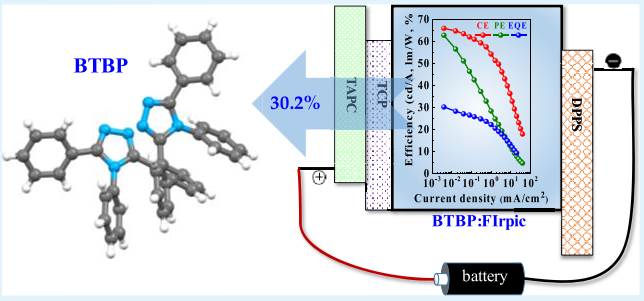

KEYWORDS: *organic light-emitting diode, wide bandgap, bipolar, electron transport, sky-blue phosphorescence*

1. INTRODUCTION

Blue phosphorescence is one of the most important issues in the development of organic light-emitting diode (OLED) display and lighting.[1−5] Compared to green and red phosphorescent emitters, the blue ones have much higher triplet states, thus imposing much difficulty on molecule design, carrier-transporting characteristics, and reliability.[6−9] For the past few years, efficient blue phosphor emitters like iridium(III) bis[4,6-di-fluorophenyl-pyridinato-N,C^2]-picolinate (FIrpic), fac-iridium(III) tris(mesityl-2-phenyl-1*H*-imidazole) (fac-Ir(mpim)$_3$), fac-iridium(III) tris(*N*-phenyl,*N*-methyl-pyridoimidazol-2-yl) (fac-Ir(pmp)$_3$), iridium(III) tris-[3-(2,6-dimethylphenyl)-7-methylimidazo[1,2-*f*]-phenanthridine] (Ir(dmp)$_3$), iridium(III)[bis(4,6-difluoro-phenyl) pyridinato-N,$C^{2'}$-tetrakis(1-pyrazolyl)borate (FIr6), etc., have been disclosed to have an external quantum efficiency (EQE) over 20%.[10,11] Generally, to avoid backward energy transfer, host materials with triplet energy (E_T) higher than blue dopants were necessary for high efficiency.[12−16] For example, carbazole-based materials were typically used as the hosts for blue phosphor dopant (e.g., FIrpic with E_T = 2.65 eV) due to the wider triplet energy (e.g., E_T = 2.9 eV for *N*,*N*-dicarbazolyl-3,5-benzene (mCP); E_T = 2.8 eV for 3,3′-di(9*H*-carbazole-9-yl)-1,1′-biphenyl (mCBP)).[17−20] Well-known benchmark bipolar host materials mCP and mCBP have good hole-transporting characteristics and also demonstrate good efficiency performance with an EQE around 20% for the blue phosphorescent OLED.[10,21] However, typically, such a host material exhibited higher hole mobility than the electron one, which results in carrier imbalance and reduces the electroluminescence efficiency. Donor−acceptor-type bipolar organic materials were synthesized as the host of blue phosphorescent OLED for improving the efficiency and reducing the efficiency roll-off by connecting the hole-transporting unit (e.g., carbazole moiety) and electron-

Received: July 30, 2020
Accepted: October 12, 2020
Published: October 23, 2020

https://dx.doi.org/10.1021/acsami.0c13705
ACS Appl. Mater. Interfaces 2020, 12, 49895−49904

Scheme 1. Synthetic Procedure of BTBP

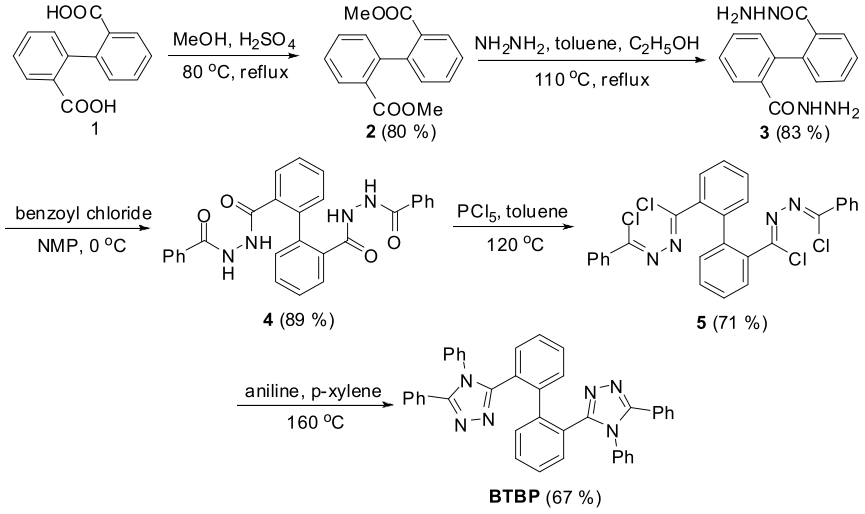

transporting unit (e.g., cyano, triazole, phosphine oxide, benzimidazole, and oxadiazole moieties).[21−26] Many bipolar host materials such as mCP, mCBP, mNBICz, UGH2, CbzBiz, DPEPO, and so on were reported with the high-efficiency OLEDs.[10,27−31] Specifically, most of these bipolar hosts exhibited a faster intrinsic hole mobility compared to the intrinsic electron one. When doped with emitters as the emitting layer (EML), the effective hole mobility of this mixture was routinely greater than electron one.[29,30] It is rare to find a bipolar host with a favorable electron-transporting behavior, which is important to contrive the carrier balance in using the hole-transporting dopant or hole-beneficial OLED structure. The carrier balance inside the emitting layer benefits the efficiency enhancement. Hence, several approaches to achieve the carrier balance in the EML were reported by introducing a mixed host (MH) by coevaporating hole- and electron-transporting hosts or a double EML structure with two adjacent hole- and electron-transporting hosts.[32−35]

In this study, a new compound, 2,2′-bis(4,5-diphenyl-(1,2,4)-triazol-3-yl)biphenyl (**BTBP**), was synthesized using an end group, triazoles, to connect with the biphenyl core because triazole derivatives are well-known electron transport materials, which have been widely used as electron-transporting layers for OLED applications, such as TAZ. However, the usage of triazole derivatives as a host was rare, especially for the blue host. For example, Adachi *et al.* reported 3-phenyl-4-(1′-naphthyl)-5-phenyl-1,2,4-triazole as a host for the $Ir(ppy)_3$ emitter. The green phosphorescent OLED showed an EQE of 15.4% and PE of 40 lm/W.[36] Su *et al.* reported a series of pyridine-TAZ hybrid molecules, with TAZ as the core and the pyridinyl groups as substituents on periphery, as the host of $Ir(ppy)_3$. The green phosphorescent OLED showed a good performance with a CE of 73.6 cd/A, PE of 72.2 lm/W, and EQE of 21.8%.[37] In our previous works, the pristine TAZ was employed as a blue host doped with an FIrpic emitter to achieve an efficient phosphorescent OLED with a CE of 45.9 cd/A and EQE of 20.2%;[21] the C2 chirality of the biphenyl core was also demonstrated to allow the stacking of electron-transporting moieties (e.g., oxadiazole) and to make the through-space interactions feasible.[38] Hence, in this study, **BTBP** was synthesized, combining the viewpoint of our above two reports, and employed as the host for blue phosphorescent OLED, which showed efficient device performances. In particular, this material possesses a large bandgap, high glass transition temperature (T_g), and high E_T of 3.1 eV. Easy synthesis, simple procedure, and cost less can be obtained. The single carrier device and time-of-flight measurement show that the material properties is bipolar with a favorable electron-transporting behavior. By suitable tuning of the device structure, a maximum current efficiency (CE_{amx}), maximum power efficiency (PE_{max}), and maximum EQE (EQE_{max}) of 65.9 cd/A, 62.8 lm/W, and 30.2%, respectively, can be obtained in our **BTBP**-based blue phosphorescent OLED.

2. EXPERIMENTS

2.1. Synthesis of BTBP (Scheme 1). Synthesis of **BTBP** is illustrated in Scheme 1.

*2.1.1. Synthesis of Dimethyl Biphenyl-2,2′-dicarboxylate (**2**).* A mixture of biphenyl-2,2′-dicarboxylic acid (**1**) (11.0 g, 45.4 mmol) in methanol (50 mL) was dripped in concentrated sulfuric acid (98%, 5 mL). The mixture was refluxed for 24 h, cooled down to the room temperature, and concentrated to give a white solid precipitate. The solid was collected and rinsed several times with methanol to afford pure solid **2** (9.9 g, 80% yield). Mp 329−330 °C. ^{1}H NMR (400 MHz, $CDCl_3$, δ) (Figure S1): 8.00 (dd, J_1 = 7.7 Hz, J_2 = 0.92 Hz, 2H), 7.51 (td, J_1 = 7.5 Hz, J_2 = 1.2 Hz, 4H), 7.19 (d, J = 7.7 Hz, 2H), 3.59 (s, 3H); ^{13}C NMR (100 MHz, $CDCl_3$, δ) (Figure S2): 167.28, 143.17, 131.36, 130.09, 129.73, 129.26, 127.06, 51.68; MS (FAB) 271 (M + H$^+$); HRMS (FAB) calcd for $C_{16}H_{15}O_4$, 271.0970 (M + H$^+$); obsd., 271.0976 (Figure S3).

*2.1.2. Synthesis of Biphenyl-2,2′-dicarbohydrazide (**3**).* Compound **2** (5.0 g, 18.5 mmol), ethanol (95%, 20 mL), toluene (20 mL), and hydrazine (100%, 18 mL, 250 mmol) were mixed and refluxed under nitrogen for 24 h. After reaction, the reaction mixture was concentrated under reduced pressure. The product was precipitated as a white solid in ethanol (95%). The solid was rinsed with ethanol (95%) and toluene to give pure white solid **3** (4.2 g, 83% yield). Mp 202−203 °C. ^{1}H NMR (400 MHz, DMSO-d_6, δ) (Figure S4): 9.61 (s, 2H), 7.47−7.40 (m, 6H), 7.06−7.03 (m, 2H), 4.24 (s, 4H); ^{13}C NMR (100 MHz, DMSO-d_6, δ) (Figure S5): 168.26, 138.82, 134.90, 129.32, 129.24, 127.51, 127.41; MS (FAB) 271 (M + H$^+$); HRMS (FAB) calcd for $C_{14}H_{15}O_2N_4$, 271.1195 (M + H$^+$); obsd., 271.1197 (Figure S6).

*2.1.3. Synthesis of N′2,N′2′-Dibenzoylbiphenyl-2,2′-dicarbohydrazide (**4**).* To a solution of **3** (3.0 g, 11 mmol) in NMP (30 mL) was slowly injected benzoyl chloride (2.58 mL, 22.2 mmol) at 0 °C under a nitrogen atmosphere. The mixture was stirred for 24 h at room temperature and slowly dripped into water. The precipitated solid was collected and rinsed twice with hot ethanol and once with

https://dx.doi.org/10.1021/acsami.0c13705
ACS Appl. Mater. Interfaces 2020, 12, 49895−49904

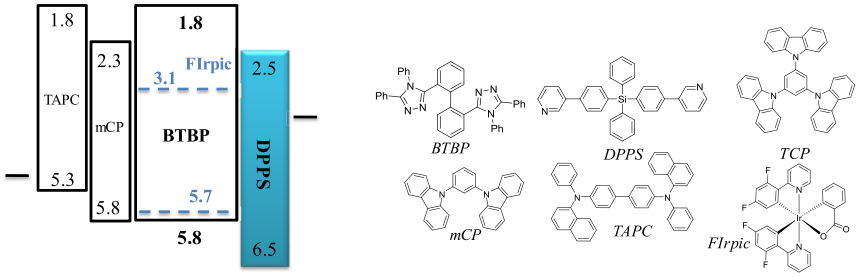

Figure 1. Layer structure and energy diagrams of OLED and chemical structures of organic materials.

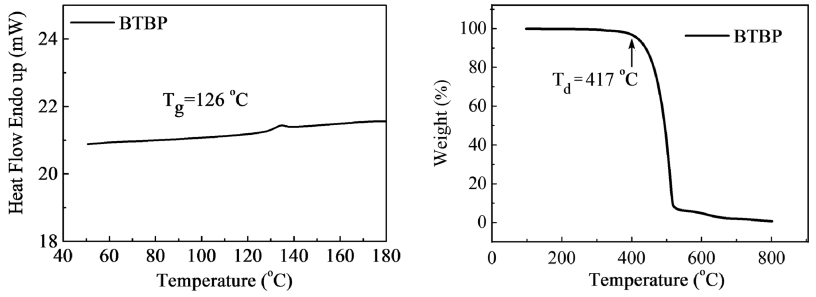

Figure 2. (a) DSC and (b) TGA analyses of **BTPB**.

ether to afford **4** as a white solid (4.7 g. 89% yield). Mp 294−295 °C. ^{1}H NMR (400 MHz, DMSO-d_6, δ) (Figure S7): 10.46 (s, 2H), 10.40 (s, 2H), 7.84 (dd, J_1 = 8.4 Hz, J_2 = 1.4 Hz, 4H), 7.65−7.64 (m, 2H), 7.57−7.44 (m, 10H), 7.25−7.24 (m, 2H); ^{13}C NMR (100 MHz, DMSO-d_6, δ) (Figure S8): 168.24, 165.57, 138.93, 134.08, 132.19, 131.85, 130.29, 129.87, 128.38, 127.88, 127.49; MS (FAB) 479 (M + H$^+$); HRMS (FAB) calcd for $C_{28}H_{23}O_4N_4$, 479.1719 (M + H$^+$); obsd., 479.1708 (Figure S9).

*2.1.4. Synthesis of (2Z,2′Z,N′2Z,N′2′Z)-N′2,N′2′-Bis(chloro-(phenyl)methylene)biphenyl-2,2′-bis(carbohydrazonoyl) dichloride (**5**).* A mixture of **4** (2 g, 4.2 mmol) and PCl_5 (3.7 g, 17.9 mmol) in toluene (16 mL) was refluxed for 3 h under N_2. The reaction was quenched by addition of water at room temperature. The product was extracted several times with toluene. The collected organic layer was dried over anhydrous $MgSO_4$ and concentrated under reduced pressure to give a white solid that was further recrystallized from CH_2Cl_2/EtOH to pure **5** (1.6 g, 71% yield). Mp 124−125 °C; ^{1}H NMR (400 MHz, $CDCl_3$, δ) (Figure S10): 8.01 (d, J = 7.56 Hz, 4H), 7.86 (d, J = 7.96 Hz, 2H), 7.51−7.38 (m, 12H); ^{13}C NMR (100 MHz, $CDCl_3$, δ) (Figure S11): 143.58, 143.50, 140.14, 133.87, 133.53, 131.65, 131.52, 130.37, 130.33, 128.48, 128.40, 127.60; MS (FAB) 553 (M + H$^+$) (Figure S12); HRMS (FAB) calcd for $C_{28}H_{19}N_4Cl_4$, 551.0334 (M + H$^+$); obsd., 551.0350.

*2.1.5. Synthesis of 2,2′-Bis(4,5-diphenyl-4H-1,2,4-triazol-3-yl)-biphenyl (**BTBP**).* Compound **5** (2.0 g, 3.6 mmol) and aniline (2.00 mL, 21.7 mmol) in *p*-xylene (28 mL) were heated at 160 °C under N_2 for 24 h. The mixture was concentrated under reduced pressure to give a crude solid. The solid was rinsed with EtOAc and recrystallized from CH_2Cl_2/EtOH to obtain white pure **BTBP** (1.4 g, 67% yield). Mp 309−311 °C; ^{1}H NMR (400 MHz, CD_2Cl_2, δ) (Figure S13): 7.48 (d, J = 7.7 Hz, 2H), 7.39−7.31 (m, 6H), 7.29−7.25 (m, 6H), 7.14−7.06 (m, 4H), 6.96 (t, J = 7.7 Hz, 4H), 6.44 (t, J = 8.2 Hz, 6H); ^{13}C NMR (100 MHz, CD_2Cl_2, δ) (Figure S14): 154.30, 154.01, 140.40, 135.03, 132.56, 132.43, 130.74, 129.89, 129.81, 129.44, 128.71, 128.32, 128.28, 127.82, 126.81, 126.29; MS (FAB) 593 (M + H$^+$); HRMS (FAB) calcd for $C_{40}H_{28}N_6$, 592.2375 (M + H$^+$); obsd., 592.2375 (Figure S15). Anal. calcd for $C_{40}H_{28}N_6$: C, 77.28; H. 4.94; N, 12.87; found: C, 77.23; H, 4.912; N, 12.903.

2.2. OLED Fabrication. Figure 1 shows the layer structures and energy levels of the blue phosphorescent OLEDs. Our devices were fabricated on indium tin oxide (ITO) glass substrates treated by O_2 plasma prior to thin-film deposition. Here, the layer structure of OLED used was 50 nm 4,4′-cyclohexylidenebis[*N*,*N*-bis(4-methylphenyl)benzenamine] (TAPC)/10 nm *m*CP/30 nm **BTBP**:*x* %FIrpic/*y*-nm diphenylbis(4-(pyridin-3-yl)phenyl)silane (DPPS)/1.2 nm LiF/100 nm Al, where TAPC and *m*CP were the first and second hole transport layers (HTLs), respectively, **BTBP** was used as the host and doped with a sky-blue dopant FIrpic as the EML, DPPS was the electron transport layer (ETL), and LiF and Al were used as the electron injection layer and cathode, respectively. In particular, the EML neighboring materials, mCP and DPPS, possess E_T values of 2.9 and 2.7 eV, which are greater than that of FIrpic (2.65 eV) to block the triplet exciton diffusion. Moreover, a faster hole mobility material, 1,3,5-tris(carbazol-9-yl)benzene (TCP), possesses similar energy-level properties like mCP, employed to replace the mCP HTL for the device optimization process. All the thin-film deposition processes were conducted via thermal evaporation in a high vacuum chamber (~8 × 10^{-6} torr). Chemical structures and energy diagrams of all organic materials are also shown in Figure 1. After thin-film deposition, OLEDs were transferred into a glove box with O_2 and H_2O less than 1 ppm for encapsulation. For evaluating the hole- and electron-transport characteristics, hole- and electron-only devices (HOD and EOD) were also fabricated. The HOD structure was glass substrate/Al (50 nm)/MoO_3 (10 nm)/mCP (10 nm)/**BTBP** (50 nm)/mCP (10 nm)/MoO_3 (10 nm)/Al (50 nm). The MoO_3 (10 nm)/mCP (20 nm) stack was used to block electrons and ensure the hole-only carrier transport. On the other hand, we used 4,7-diphenyl-1,10-phenanthroline (BPhen) exhibiting high electron mobility as the hole-blocking layer in our EOD device, which was glass substrate/Al (50 nm)/LiF (1.2 nm)/BPhen (10 nm)/**BTBP** (50 nm)/BPhen (10 nm)/LiF (1.2 nm)/Al (50 nm). In addition, charge-transporting properties of vacuum-deposited films of **BTBP** were also tested using the time-of-flight (ToF) technique.[39] In the ToF setup, time-resolved excitation of samples through the ITO electrode was performed using the Nd:YAG laser EKSPLA NL300 with the wavelength of 355 nm and pulse duration of 6 ns (Figure S16a). Since films of **BTBP** are transparent at the emission wavelength of the laser used, a layer of pentacene as an absorber was deposited. Thus, ITO/pentacene (250 nm)/**BTBP** (2 μm)/Al was the structure of ToF samples. Charges were generated under the laser excitation in the layer of pentacene. Then, holes or electrons were transported through the layer of **BTBP**

https://dx.doi.org/10.1021/acsami.0c13705
ACS Appl. Mater. Interfaces 2020, 12, 49895−49904

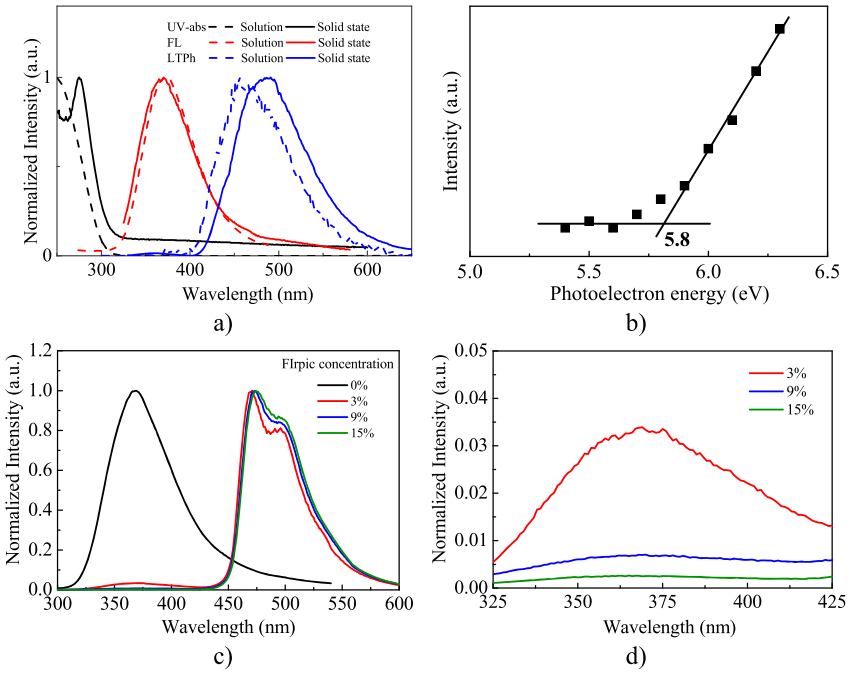

Figure 3. (a) Absorption, fluorescence, and low-temperature phosphorescence spectra of **BTBP** solution and thin film; (b) photoelectron spectrum of **BTBP** thin film; (c) PL spectra of **BTBP** thin film doped with different FIrpic concentrations from 0 to 15% in (a) a full wavelength range (300−600 nm) and (d) zoom-in short wavelength region (325−425 nm).

depending on the polarity of external electric field applied to the sample using the electrometer Keithley 6517B (Figure S16a). ToF photocurrent transients for holes or electrons at different electric fields were recorded using a Tektronix TDS 3032C oscilloscope. To obtain carrier transit times (t_{tr}), ToF photocurrent transients were plotted in log−log plots (Figure S16b,c). Charge mobilities at different electric fields were calculated by the usual formula $\mu = d^2/(U \times t_{tr})$, where d is the layer thickness, and U is the surface potential at the moment of illumination. Luminance−voltage−current density measurements were obtained via a Keithley 2400 multisource meter and Minolta CS-1000 spectrometer, whose setup was also used to record both the driving current and angular emission spectra to obtain the EQE value.[40] A Hitachi F-4500 fluorescence spectrophotometer with the excitation wavelength at 270 nm was used for obtaining the photoluminescence (PL) spectra. The values of highest occupied molecular orbital (HOMO) in Figure 1 were obtained from low-energy photoelectron spectra measurement (Riken-Keiki AC-2 spectrometer) with organic thin films deposited on a glass substrate. The lowest unoccupied molecular orbital (LUMO) was deduced from HOMO levels and the absorption spectra were taken using a Hitachi U4100 spectrometer.

3. RESULTS AND DISCUSSIONS

3.1. BTBP Properties. From differential scanning calorimetry (DSC) and thermogravimetric analysis (TGA) measurements (Figure 2), the T_g and decomposition temperature (T_d) of **BTBP** are 126 and 417 °C, respectively. Such a high T_g value is essential for achieving long operation lifetime of an OLED.

Figure 3a presents the UV−Vis absorption, fluorescence (FL), and low-temperature phosphorescence spectra (LTPh at 77 K) of **BTBP** measured in THF and in solid-state film state. The absorption peaked at 248 nm is attributed to the $\pi-\pi^*$ transitions. Observation of almost identical absorption and emission patterns for **BTBP** in solution and in film state suggested that intermolecular $\pi-\pi$ stacking effects are small in the matrix. The energy bandgap of 4.0 eV is estimated on the basis of the onset of the solid-state absorption spectrum. A high degree of spectral overlap between the fluorescence emission of **BTBP** and the MLCT absorption of FIrpic allows effective energy transfer from **BTBP** to FIrpic. The LTPh reveals E_T values of 3.1 and 3.0 eV for **BTBP** solution and solid-state film, respectively, which are high enough to prevent the occurrence of energy back transfer, and therefore, **BTBP** can be considered as a useful host material for FIrpic (E_T of 2.65 eV) in blue phosphorescent OLED application. The HOMO energy level of 5.8 eV of **BTBP** can be obtained from the photoelectrical spectrum (Figure 3b). After subtracting the energy bandgap of 4.0 eV, the LUMO energy level is very high, reaching 1.8 eV (Figure 1). Figure 3c shows the PL spectra of **BTBP** thin film on glass substrates doped by FIrpic with different concentrations (0, 3, 9, and 15%). The emission peak of the pure **BTBP** thin film was at 369 nm. When it was doped with FIrpic, although the dopant concentration was as low as 3%, obvious FIrpic emission (peaks at 471 and 495 nm in Figure 3c) was observed. The relative intensity at a long wavelength peak (495 nm) increased with dopant concentration, which may come from trivial absorption and/or intermolecular interaction of FIrpic molecules. When enlarging the **BTBP** PL emission at a short wavelength region (peak at 369 nm) (Figure 3d), one can see the decrease in **BTBP** emission with increasing dopant concentration. It showed efficient energy transfer from **BTBP** to FIrpic when the dopant concentration was higher than 15%.

X-ray crystallography is a useful method of understanding material properties. Figure 4 shows the X-ray crystallography in different view angles and material packing of **BPTP**. **BPTP** has the torsion angle $\Phi = 53.59°$ (Figure 4a), and it has a highly twisted geometric structure. Figure 4b shows the benzene ring with a triazole ring having the torsion angle $\Phi = 52.04°$, and it may allow the benzene and triazole orbital to have some overlap and let this molecule have some intramolecular change transfer. The closest distance between two face-to-face triazole

https://dx.doi.org/10.1021/acsami.0c13705
ACS Appl. Mater. Interfaces 2020, 12, 49895−49904

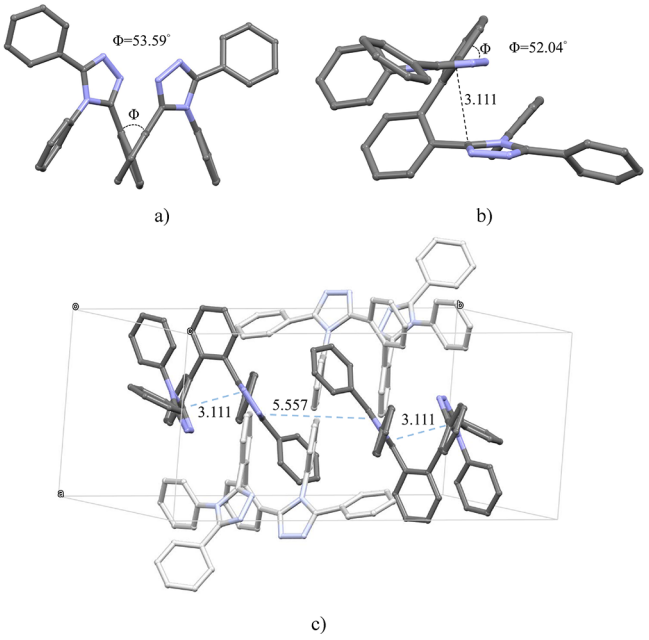

Figure 4. (a, b) X-ray crystallography analysis of **BTBP** in different view angles and (c) crystal lattice diagram of **BTBP** packing.

rings is 3.111 Å, which allows the space $\pi-\pi$ interactions. Figure 4c and Figure S17 show the molecule packing in crystal lattice; the distances between intermolecular triazole rings are 5.557 and 5.659 Å. The channel of intramolecular and intermolecular triazoles benefits the electron transportation to enhance the electron mobility, which is similar to our initial concept.

Figure 5 shows the geometry and HOMO and LUMO diagrams obtained by DFT calculations at the B3LYP/6-31G(d,p) level using Gaussian 09, Revision A.02 (Gaussian Inc., Wallingford, CT, 2016).[41,42] The energy-minimized structure of **BTBP** is nonplanar, thus reducing the $\pi-\pi$ interactions. The nonplanar structure of **BTBP** prevents its participation in the formation of excimers or exciplexes between the host and guest (or molecules from the neighboring layers). HOMO is distributed over the electron-rich side of phenyl rings, whereas LUMO is mainly localized on the triazole rings and biphenyl core. The HOMO and LUMO of the molecule partly overlap, which may lead to intramolecular charge transfer effects.[43] Such spatial distribution leads to a low LUMO energy level of −0.99 eV, which is favorable for the efficient electron injection and efficient electron transport. The calculated HOMO−LUMO gap for the host material is of 4.83 eV and is larger than the experimental one, obtained from the UV−Vis absorption spectra.

Figure 6a shows the $J-E$ characteristics of HOD and EOD of **BTBP**. Under a low electric field (<5 × 10^5 V/cm), the current density increased linearly with increasing electric field, which came from free carrier conduction or leakage current. Also, the current density values were quite similar for HOD and EOD. When increasing the electric field higher than 5 × 10^5 V/cm, the current density of EOD increased dramatically and was orders of magnitude higher than that of HOD, which showed that **BTBP** was mainly an electron transport material. We can make a rough estimation of electron-transporting capability for real OLED application. For example, when applying 6 V on 30 nm EML, it corresponded to ∼2 × 10^6 V/cm in electric field, and **BTBP** provided the (electron-only) current density of 10 mA/cm^2. Carrier mobility in an organic thin film was typically modeled with the following Poole−Frenkel equation.

$$\mu = \mu_0 \exp(\beta E^{0.5}) \quad (1)$$

where μ is the carrier (electron or hole) mobility, μ_0 is the field-free mobility, β is the Poole−Frenkel constant, and E is the electric field. With increasing electric field, the carrier mobility increased.

To precisely obtain electric field dependences of hole and electron mobilities of **BTBP**, the ToF was used. By the ToF experiment, it is proved that the **BTBP** layer exhibits higher electron mobility in comparison to hole mobility at the same electric fields (Figure 6b). For example, hole and electron mobilities of 2.9 × 10^{-5} and 5.8 × 10^{-5} $cm^2 \cdot V^{-1} \cdot s^{-1}$, respectively, were observed at the electric field of 1.1 × 10^6 $V \cdot cm^{-1}$. It should be noted that electric field dependences of hole and electron mobilities of **BTBP** contained certain errors since it was difficult to determine transit times due to the very strong charge dispersity in the **BTBP** layer evident from current transients (Figure S16b,c). For the same reason, charge mobilities were detected only at very high electric fields (>7 × 10^5 $V \cdot cm^{-1}$). Nevertheless, it was previously demonstrated that hosts with mobility reaching 10^{-5} $cm^2 \cdot V^{-1} \cdot s^{-1}$ showed good performances in blue OLEDs.[44,45] Electric field dependences of hole and electron mobilities of **BTBP** were well described by the Poole−Frenkel model (eq 1). Parameters μ_0 and β are presented in Figure 6b. A higher value of β for electrons demonstrates a faster increase in electron mobility with increasing electric fields in comparison to that of holes. These findings are in good agreement with the space-charge-limited current−voltage measurements described above.

3.2. Device Performance. *3.2.1. ETL Modification.* In an OLED, the electron mobility of ETL was typically much lower than hole one of HTL. In addition, the wide-angle interference also depended on the length between the emissive dipole and reflective electrode (Al cathode in this case). These two factors made the ETL thickness very critical. Hence, we chose the dopant concentration (x%) at 15% because of the promised energy transfer (Figure 3d) and varied the ETL thickness, y

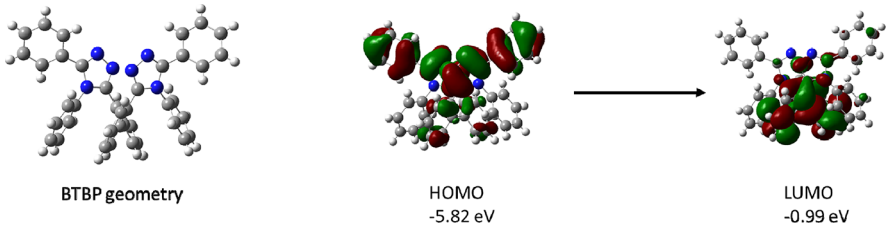

Figure 5. Geometry and HOMO and LUMO diagrams of **BTBP**.

https://dx.doi.org/10.1021/acsami.0c13705
ACS Appl. Mater. Interfaces 2020, 12, 49895−49904

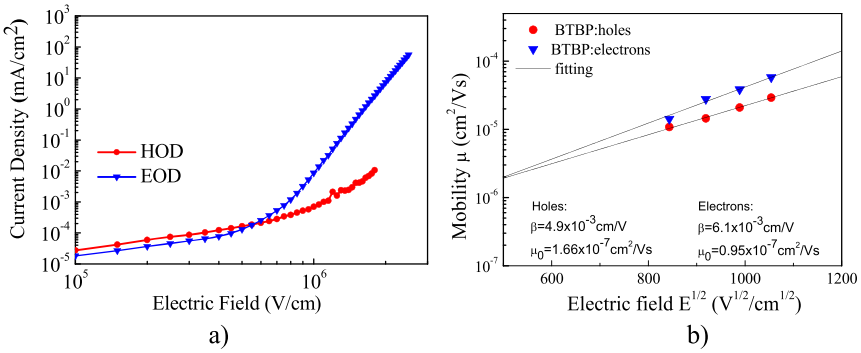

Figure 6. (a) Space-charge-limited current−voltage dependences for the HOD and EOD devices based on **BTBP**; (b) hole and electron mobilities vs electric fields for **BTBP** layers obtained by the ToF experiment.

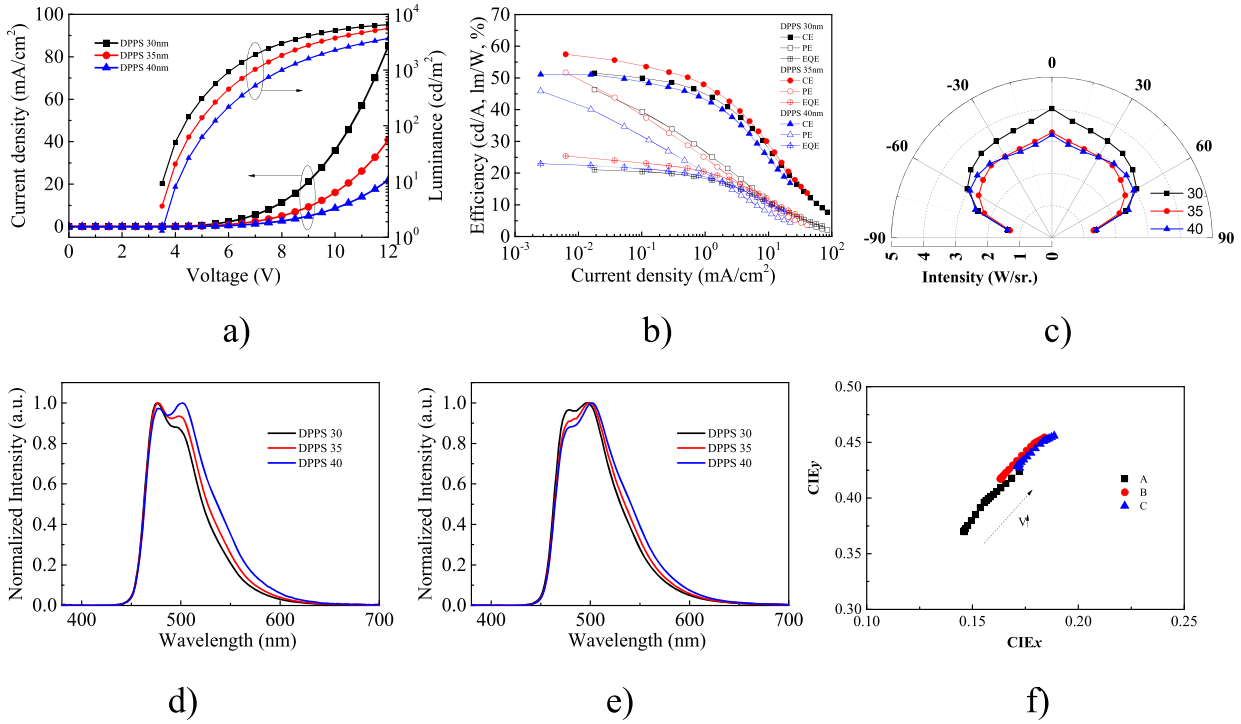

Figure 7. (a) *J*−*L*−*V*, (b) EL efficiencies−*J*, (c) angular emission patterns, EL spectra at (d) 4 V and (e) 10 V, and (f) color coordinates of devices A−C (*y* = 30, 35 and 40 nm).

Table 1. Electroluminescence Performance of OLEDs with Various ETL Thicknesses (Devices A−C), Various Dopant Concentrations (Devices D−F), and Enlarged EML Thickness (Device G)

device	voltage[a] (V)	luminance[b] (cd/m²)	$CE_{max}CE_{1000}$[c] (cd/A)	$PE_{max}PE_{1000}$[c] (lm/W)	$EQE_{max}EQE_{1000}$[c] (%)
A	6.9	6571	51.6/40.4	46.4/20.8	21.1/16.1
B	8.0	5602	57.2/42.9	51.5/19.3	25.4/18.1
C	9.0	3692	51.1/37.8	45.9/16.1	22.9/14.8
D	7.4	7322	57.9/46.0	51.9/22.8	25.5/19.6
E	7.3	7948	61.1/49.0	55.0/24.8	27.2/21.8
F	6.6	10,180	53.1/44.1	47.7/24.2	22.2/18.0
G	8.0	7135	65.9/50.5	62.8/23.7	30.2/20.0

[a]At *J* of 5 mA/cm. [b]At *V* of 12 V. [c]max: maximum; 1000: 1000 cd/m².

factor, from 30 to 40 nm with a 5 nm interval as devices A−C. Figure 7a shows the *J*−*V* characteristics of devices A−C. Obviously, the driving voltage increased with the thicker ETL thickness (Table 1), which describes that certain voltage drops on the ETL. Considering the efficiency performances (Figure 7b), it can be easily identified that the optimized ETL thickness is 35 nm. Among devices A−C, device B shows favorable CE_{max}, PE_{max}, and EQE_{max} of 57.2 cd/A, 51.5 lm/W, and 25.4%, respectively. An obvious efficiency roll-off phenomenon can be observed for these FIrpic-based OLEDs because the main EML suffers the severe effects of triplet-triplet annihilation and triplet-polaron annihilation at high

https://dx.doi.org/10.1021/acsami.0c13705
ACS Appl. Mater. Interfaces 2020, 12, 49895−49904

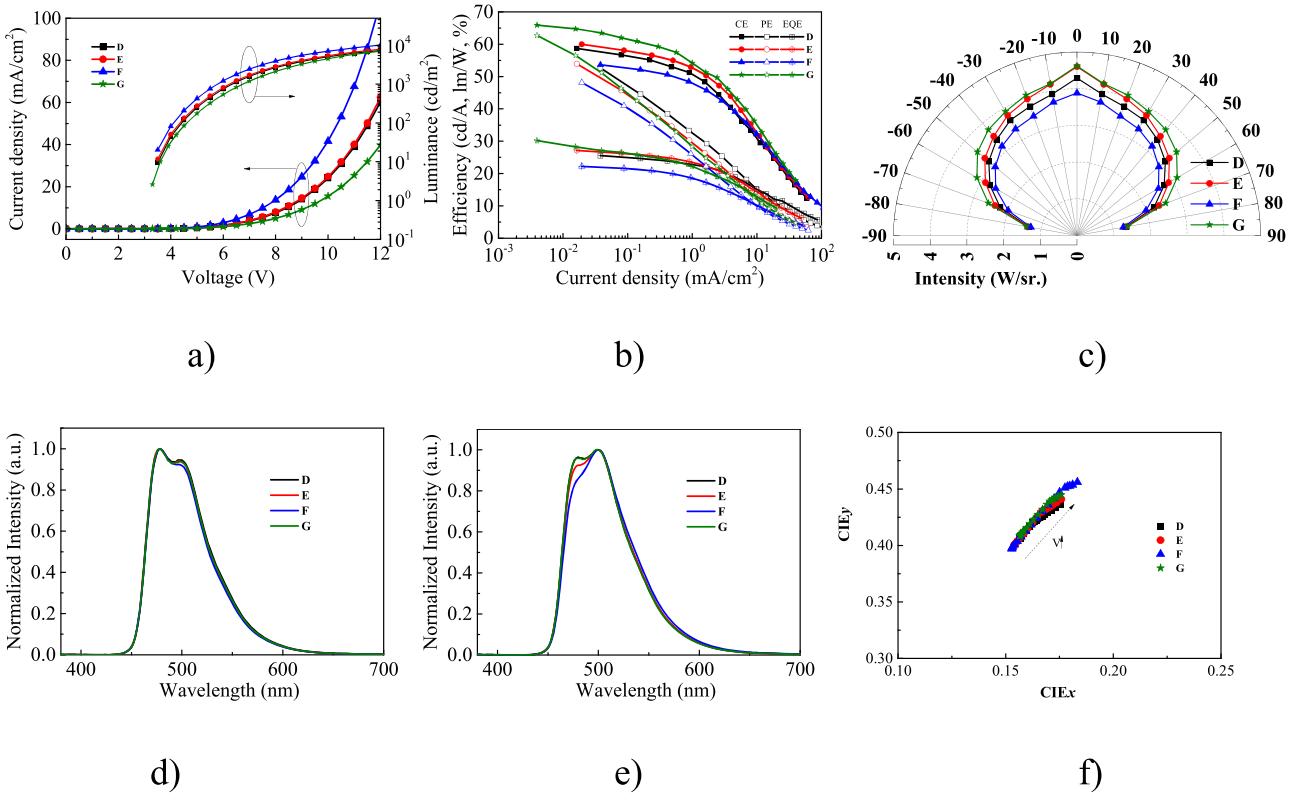

Figure 8. (a) *J*−*L*−*V*, (b) EL efficiencies−*J*, (c) angular emission patterns, EL spectra at (d) 4 V and (e) 10 V, and (f) color coordinates of devices D−F (x = 18, 21, and 24%, respectively).

current density and high brightness. This efficiency roll-off can be further improved by carefully managing triplet excitons in the EML,[46,47] but it is not the scope of this study. In Figure 7c, device B exhibits the greater emission intensity recoded in various view angles, especially in the angles from 0° to ±60°. Figure 7d,e shows the EL spectra of devices A−C at 4 and 10 V, respectively. One can see that the relative intensity of long wavelength increased with increasing ETL thickness because the increase in distance between the recombination zone and cathode resulted in a cavity resonance effect. With increasing driving voltage, the recombination zone shifted farther away from the cathode, leading to the increase in the long wavelength of the EL spectral profiles. These also describe the greenshift movement of color coordinates in the CIE diagram (Figure 7f). For example, the color coordinate of the device B moves from (0.163, 0.417) to (0.179, 0.449) when the driving voltage increases from 4 to 10 V.

3.2.2. EML Modification. To upgrade the device performance greater than device B (15% FIrpic), a series of devices D−F with increasing FIrpic concentrations (x%) in volume ratios of 18, 21, and 24%, respectively, were fabricated, their electroluminance (EL) performances were measured as shown in Figure 8, and their characteristics are summarized in Table 1. In Figure 8a, the *J*−*V* curves of devices D−F showed that the driving voltage decreased with increasing dopant concentrations. This is because the hole mobility was much lower than the electron mobility of **BTBP**, as shown in Figure 6, which resulted in the difficulty in hole transporting in the EML. Hence, the heavy doping ratio of FIrpic constructed a path beneficial for hole transportation and then reduced the driving voltage. Figure 8b shows the efficiencies versus current density curves of devices D−F. The highest CE, PE, and EQE of 61.1 cd/A, 55.0 lm/W, and 27.2%, respectively, were obtained at device E (21% FIrpic) under 3.5 V driving voltage, as shown in Table 1. In particular, this device also exhibits the enhanced EL intensity in various view angles from 0° to ±80° (Figure 8c). In comparison with device B (15% FIrpic), the increasing FIrpic concentration resulted in the longer hole-transporting path in the EML of devices D−F, leading to greater resonance in blue band (with a peak near 474 nm) of the EL spectrum no matter at 4 or 10 V (Figure 8d,e). Similar to the carrier dynamics and optical cavity effects in above devices A−C (Figure 7), with increasing driving voltage, the recombination zone shifted farther away from the cathode, leading to the increase in the long wavelength of the EL spectral profiles. These also describe the greenshift movement of color coordinates in the CIE diagram (Figure 8f). For example, the color coordinate of device E moves from (0.154, 0.400) to (0.169, 0.433) when the driving voltage increases from 4 to 10 V.

In addition, several approaches in the EML modification such as thickness adjustment (Figure 8), gradient dopant, and double EML structure (Figure S18) were employed to further optimize the device efficiency. To accelerate the hole transportation, a faster hole mobility HT material, TCP, was employed to replace the mCP. Device G was fabricated and exhibited an efficiency improvement by introducing the 10 nm TCP HTL and also enlarging the EML thickness to 40 nm, which may result in the favorable carrier balance compared with that of other approaches. Device G showed a degraded *J*−*L*−*V* curve due to the thicker device structure. Although with the lagged *J*−*L*−*V* behavior (Figure 8a), the process of carrier injection, transportation, and recombination to become a photon was efficient, especially under a low driving *J*. At *J* ≈

https://dx.doi.org/10.1021/acsami.0c13705
ACS Appl. Mater. Interfaces 2020, 12, 49895−49904

0.02 mA/cm^2 (Figure 8b), device G exhibited a greater efficiency (CE_{max} of 64.7 cd/A, PE_{max} of 56.5 lm/W, and EQE_{max} of 28.3%) than device E. In a case of lower J = 0.004 mA/cm^2, device G with a luminance of 2.6 cd/m^2 showed maximum efficiency performances with a CE_{max} of 65.9 cd/A, PE_{max} of 62.8 lm/W, and EQE_{max} of 30.2%. This high device efficiency could be also confirmed by the high photoluminescence quantum yield value of 92.9% for the **BTBP**:21%FIrpic thin film, which was the EML inside the device. The EL spectra at 4 and 10 V (Figure 8d,e) and the color coordinates (Figure 8f) were similar with those of devices D−F. In addition, to realize the carrier transportation and main carrier recombination zone inside the EML of device G (Figure S19), a series of OLEDs with the undoped and partial-doped EMLs were fabricated and their results described that the whole EML was dominated the device efficiency and the main recombination zone was located toward HTL, which is because the **BTBP** host belongs to the electron-favorable bipolar behavior.

4. CONCLUSIONS

A wide bandgap organic compound, **BTBP**, was successfully synthesized by conjugating two electron-transporting triazole moieties on a hole-transporting biphenyl core. The material properties of **BTBP** were characterized to have a wide bandgap of 4 eV, high triplet energy over 3 eV, HOMO of 5.8 eV, LUMO of 1.8 eV, high glass transition temperature of 126 °C, and ultrahigh decomposition temperature of 417 °C. In addition, this **BTBP** showed the electron-favorable bipolar behavior with close hole and electron mobilities of 2.9×10^{-5} and 5.8×10^{-5} cm^2·V^{-1}·s^{-1}, respectively, at a low electric field of 1.1×10^6 V·cm^{-1}. In particular, this **BTBP** exhibits bipolar behavior at a low electric field and electron-transporting behavior at a high electric field. We utilized this **BTBP** as a host and demonstrated a blue phosphorescent OLED to achieve the high-efficiency performances with CE_{max}, PE_{max}, and EQE_{max} of 65.9 cd/A, 62.8 lm/W, and 30.2%, respectively.

■ ASSOCIATED CONTENT

Supporting Information

The Supporting Information is available free of charge at https://pubs.acs.org/doi/10.1021/acsami.0c13705.

Crystallographic data of **BTBP** (CIF)

NMR, HRMS, and mass of compounds; crystal lattice packing; ToF setup and measurement signals; device optimization utilizing a gradient dopant and double EMLs; main recombination zone probing (PDF)

■ AUTHOR INFORMATION

Corresponding Authors

Man-kit Leung − *Department of Chemistry, National Taiwan University, Taipei 10617, Taiwan;* orcid.org/0000-0002-3297-9087; Email: mkleung@ntu.edu.tw

Tien-Lung Chiu − *Department of Electrical Engineering, Yuan Ze University, Taoyuan 32003, Taiwan;* orcid.org/0000-0002-0631-660X; Email: tlchiu@saturn.yzu.edu.tw

Authors

Jiun-Haw Lee − *Graduate Institute of Photonics and Optoelectronics and Department of Electrical Engineering, National Taiwan University, Taipei 10617, Taiwan;* orcid.org/0000-0003-3888-0595

Chia-Hsun Chen − *Graduate Institute of Photonics and Optoelectronics and Department of Electrical Engineering and Department of Chemistry, National Taiwan University, Taipei 10617, Taiwan*

Bo-Yen Lin − *Graduate Institute of Photonics and Optoelectronics and Department of Electrical Engineering, National Taiwan University, Taipei 10617, Taiwan; Department of Electrical Engineering, Yuan Ze University, Taoyuan 32003, Taiwan*

Yi-Hsin Lan − *Graduate Institute of Photonics and Optoelectronics and Department of Electrical Engineering, National Taiwan University, Taipei 10617, Taiwan*

Yi-Mei Huang − *Department of Chemistry, National Taiwan University, Taipei 10617, Taiwan*

Nai-Jing Chen − *Department of Chemistry, National Taiwan University, Taipei 10617, Taiwan*

Jau-Jiun Huang − *Department of Chemistry, National Taiwan University, Taipei 10617, Taiwan*

Dmytro Volyniuk − *Department of Polymer Chemistry and Technology, Kaunas University of Technology, LT-50254 Kaunas, Lithuania;* orcid.org/0000-0003-3526-2679

Rasa Keruckiene − *Department of Polymer Chemistry and Technology, Kaunas University of Technology, LT-50254 Kaunas, Lithuania*

Juozas Vidas Grazulevicius − *Department of Polymer Chemistry and Technology, Kaunas University of Technology, LT-50254 Kaunas, Lithuania;* orcid.org/0000-0002-4408-9727

Yuh-Renn Wu − *Graduate Institute of Photonics and Optoelectronics and Department of Electrical Engineering, National Taiwan University, Taipei 10617, Taiwan*

Complete contact information is available at: https://pubs.acs.org/10.1021/acsami.0c13705

Author Contributions

J.-H.L., C.-H.C., B.-Y.L., and Y.-H.L. were in charge of the material investigations, device structure design, fabrications, characterization measurement, and data analysis. M.-k.L., Y.-M.H., N.-J.C., and J.-J.H. were in charge of molecule design and synthesis. D.V., R.K., and J.V.G. were in charge of DFT calculations and ToF measurement. Y.-R.W. carried out mobility simulation fitting from EOD and HOD behavior. T.-L.C. conceived the project, analyzed the data, and handled the paper preparation and submission.

Notes

The authors declare no competing financial interest.

■ ACKNOWLEDGMENTS

This work was supported by the Ministry of Science and Technology (MOST), Taiwan, under grants MOST 109-2634-F-002-042, 108-3017-F-002-002, 108-2221-E-155-051-MY3, 108-2912-I-155-504, 108-2811-E-155-504, 107-2221-E-155-058-MY3, 107-2221-E-002-156-MY3, 107-2221-E-155-027, 107-3113-E-155-001-CC2, 106-3113-E-155-001-CC2, 106-2221-E-155-036, 106-2923-E-155-002-MY3, 106-2923-E-002-004-MY3, 109-2221-E-002-196-MY2, 106-2221-E-002-164-MY3, 105-2221-E-002-130-MY3, the Ministry of Education (MOE) Taiwan grant 108L9006, and the MEGA Project, which has received funding from the European Union's Horizon 2020 Research and Innovation Programme under the Marie Skłodowska-Curie grant agreement no. 823720.

REFERENCES

(1) Ho, C.-L.; Wong, W.-Y. Small-Molecular Blue Phosphorescent Dyes for Organic Light-Emitting Devices. *New J. Chem.* **2013**, *37*, 1665−1683.

(2) Sasabe, H.; Kido, J. Development of High Performance OLEDs for General Lighting. *J. Mater. Chem. C* **2013**, *1*, 1699−1707.

(3) Lee, J.-H.; Chen, C.-H.; Lee, P.-H.; Lin, H.-Y.; Leung, M.-K.; Chiu, T.-L.; Lin, C.-F. Blue Organic Light-Emitting Diodes: Current Status, Challenges, and Future Outlook. *J. Mater. Chem. C* **2019**, *7*, 5874−5888.

(4) Mao, H.-T.; Li, G.-F.; Shan, G.-G.; Wang, X.-L.; Su, Z.-M. Recent Progress in Phosphorescent Ir(III) Complexes for Nondoped Organic Light-Emitting Diodes. *Coord. Chem. Rev.* **2020**, *413*, 213283.

(5) Arai, H.; Sasabe, H.; Nakao, K.; Masuda, Y.; Kido, J. Spirobiacridine-Based Host Material for Highly Efficient Blue Phosphorescent Organic Light-Emitting Devices. *Chem. Lett.* **2020**, *49*, 228−231.

(6) Holmes, R. J.; D'Andrade, B. W.; Forrest, S. R.; Ren, X.; Li, J.; Thompson, M. E. Efficient, Deep-Blue Organic Electrophosphorescence by Guest Charge Trapping. *Appl. Phys. Lett.* **2003**, *83*, 3818.

(7) Tsang, D. P.-K.; Chan, M.-Y.; Tam, A. Y.-Y.; Yam, V. W.-W. Host Engineering for Improving the Performance of Blue Phosphorescent Organic Light-Emitting Devices. *Org. Electron.* **2011**, *12*, 1114−1119.

(8) Xiao, L.; Chen, Z.; Qu, B.; Luo, J.; Kong, S.; Gong, Q.; Kido, J. Recent Progresses on Materials for Electrophosphorescent Organic Light-Emitting Devices. *Adv. Mater.* **2011**, *23*, 926−952.

(9) Zhang, C.; Liu, R.; Zhang, D.; Duan, L. Progress on Light-Emitting Electrochemical Cells Toward Blue Emission, High Efficiency, and Long Lifetime. *Adv. Funct. Mater.* **2020**, *30*, 1907156.

(10) Zhang, Y.; Lee, J.; Forrest, S. R. Tenfold Increase in the Lifetime of Blue Phosphorescent Organic Light-Emitting Diodes. *Nat. Commun.* **2014**, *5*, 5008.

(11) Zysman-Colman, E. *Iridium(III) in Optoelectronic and Photonics Applications*; John Wiley & Sons Ltd.: Chichester 2017.

(12) Tokito, S.; Iijima, T.; Suzuri, Y.; Kita, H.; Tsuzuki, T.; Sato, F. Confinement of Triplet Energy on Phosphorescent Molecules for Highly-Efficient Organic Blue-Light-Emitting Devices. *Appl. Phys. Lett.* **2003**, *83*, 569.

(13) Ren, X.; Li, J.; Holmes, R. J.; Djurovich, P. I.; Forrest, S. R.; Thompson, M. E. Ultrahigh Energy Gap Hosts in Deep Blue Organic Electrophosphorescent Devices. *Chem. Mater.* **2004**, *16*, 4743−4747.

(14) Chopra, N.; Lee, J.; Zheng, Y.; Eom, S. H.; Xue, J.; So, F. High Efficiency Blue Phosphorescent Organic Light-Emitting Device. *Appl. Phys. Lett.* **2008**, *93*, 143307.

(15) Xiao, L.; Su, S.-J.; Agata, Y.; Lan, H.; Kido, J. Nearly 100% Internal Quantum Efficiency in an Organic Blue-Light Electrophosphorescent Device Using a Weak Electron Transporting Material with a Wide Energy Gap. *Adv. Mater.* **2009**, *21*, 1271−1274.

(16) Cho, Y. J.; Lee, J. Y. Tetraphenylsilane-Based High Triplet Energy Host Materials for Blue Phosphorescent Organic Light-Emitting Diodes. *J. Phys. Chem. C* **2011**, *115*, 10272−10276.

(17) Lee, J.; Chopra, N.; Eom, S. H.; Zheng, Y.; Xue, J.; So, F.; Shi, J. Effects of Triplet Energies and Transporting Properties of Carrier Transporting Materials on Blue Phosphorescent Organic Light Emitting Devices. *Appl. Phys. Lett.* **2008**, *93*, 123306.

(18) Lee, J.; Lee, J. I.; Chu, H. Y. Investigation of Double Emissive Layer Structures on Phosphorescent Blue Organic Light-Emitting Diodes. *Synth. Met.* **2009**, *159*, 1460−1463.

(19) Klubek, K. P.; Tang, C. W.; Rothberg, L. J. Investigation of Blue Phosphorescent Organic Light-Emitting Diode Host and Dopant Stability. *Org. Electron.* **2014**, *15*, 1312−1316.

(20) Wei, P.; Zhao, S.; Xu, Z.; Song, D.; Qiao, B.; Wang, P.; Yang, J. Improved Carrier Injection and Balance in Solution-Processed Blue Phosphorescent Organic Light Emitting Diodes Based on Mixed Host System and Their Transient Electroluminescence. *Synth. Met.* **2019**, *252*, 15−20.

(21) Cheng, T. Y.; Lee, J. H.; Chen, C. H.; Chen, P. H.; Wang, P. S.; Lin, C. E.; Lin, B. Y.; Lan, Y. H.; Hsieh, Y. H.; Huang, J. J.; Lu, H. F.; Chao, I.; Leung, M. K.; Chiu, T. L.; Lin, C. F. Carrier Transport and Recombination Mechanism in Blue Phosphorescent Organic Light-Emitting Diode with Hosts Consisting of Cabazole- and Triazole-Moiety. *Sci. Rep.* **2019**, *9*, 3654.

(22) Li, W.; Li, J.; Liu, D.; Wang, F.; Zhang, S. Bipolar Host Materials for High-Efficiency Blue Phosphorescent and Delayed-Fluorescence OLEDs. *J. Mater. Chem. C* **2015**, *3*, 12529−12538.

(23) Kim, M. K.; Kwon, J.; Kwon, T. H.; Hong, J. I. A Bipolar Host Containing 1,2,3-Triazole for Realizing Highly Efficient Phosphorescent Organic Light-Emitting Diodes. *New J. Chem.* **2010**, *34*, 1317−1322.

(24) Zhuang, J.; Li, W.; Su, W.; Zhou, M.; Cui, Z. Novel Ternary Bipolar Host Material with Carbazole, Triazole and Phosphine Oxide Moieties for High Efficiency Sky-Blue OLEDs. *New J. Chem.* **2014**, *38*, 650−656.

(25) Chen, H. F.; Chi, L. C.; Hung, W. Y.; Chen, W. J.; Hwu, T. Y.; Chen, Y. H.; Chou, S. H.; Mondal, E.; Liu, Y. H.; Wong, K. T. Carbazole and Benzimidazole/Oxadiazole Hybrids as Bipolar Host Materials for Sky Blue, Green, and Red PhOLEDs. *Org. Electron.* **2012**, *13*, 2671−2681.

(26) Ledwon, P. Recent Advances of Donor-Acceptor Type Carbazole-Based Molecules for Light Emitting Applications. *Org. Electron.* **2019**, *75*, 105422.

(27) Pan, B.; Wang, B.; Wang, Y.; Xu, P.; Wang, L.; Chen, J.; Ma, D. A Simple Carbazole-N-Benzimidazole Bipolar Host Material for Highly Efficient Blue and Single Layer White Phosphorescent Organic Light-Emitting Diodes. *J. Mater. Chem. C* **2014**, *2*, 2466−2469.

(28) Li, Y.; Liu, J. Y.; Zhao, Y. D.; Cao, Y. C. Recent Advancements of High Efficient Donor−Acceptor Type Blue Small Molecule Applied for OLEDs. *Mater. Today* **2017**, *20*, 258−266.

(29) Huang, J. J.; Yun, L. K.; Kung, T. J.; Chen, C. L.; Lee, J. H.; Wu, Y. R.; Chiu, T. L.; Chou, P. T.; Leung, M. K. Networking Hole and Electron Hopping Paths by Y-Shaped Host Molecules: Promoting Blue Phosphorescent Organic Light Emitting Diodes. *J. Mater. Chem. C* **2017**, *5*, 3600−3608.

(30) Chang, S. Y.; Lin, G. T.; Cheng, Y. C.; Huang, J. J.; Chang, C. L.; Lin, C. F.; Lee, J. H.; Chiu, T. L.; Leung, M. K. Construction of Highly Efficient Carbazol-9-yl-Substituted Benzimidazole Bipolar Hosts for Blue Phosphorescent Light-Emitting Diodes: Isomer and Device Performance Relationships. *ACS Appl. Mater. Interfaces* **2018**, *10*, 42723−42732.

(31) Conaghan, P. J.; Matthews, C. S. B.; Chotard, F.; Jones, S. T. E.; Greenham, N. C.; Bochmann, M.; Credgington, D.; Romanov, A. S. Highly Efficient Blue Organic Light-Emitting Diodes Based on Carbene-Metal-Amides. *Nat. Commun.* **2020**, *11*, 1758.

(32) Chopra, N.; Swensen, J. S.; Polikarpov, E.; Cosimbescu, L.; So, F.; Padmaperuma, A. B. High Efficiency and Low Roll-Off Blue Phosphorescent Organic Light-Emitting Devices using Mixed Host Architecture. *Appl. Phys. Lett.* **2010**, *97*, No. 033304.

(33) Udagawa, K.; Sasabe, H.; Igarashi, F.; Kido, J. Simultaneous Realization of High EQE of 30%, Low Drive Voltage, and Low Efficiency Roll-Off at High Brightness in Blue Phosphorescent OLEDs. *Adv. Optical Mater.* **2016**, *4*, 86−90.

(34) Zhang, J.; Guan, Y.; Yang, J.; Hua, W.; Wang, S.; Ling, Z.; Lian, H.; Liao, Y.; Lan, W.; Wei, B.; Wong, W. Y. Highly-Efficient Solution-Processed Green Phosphorescent Organic Light-Emitting Diodes with Reduced Efficiency Roll-Off using Ternary Blend Hosts. *J. Mater. Chem. C* **2019**, *7*, 11109−11117.

(35) Kim, D. S.; Lee, K. H.; Lee, J. Y. Novel Positive Polaron Stabilizing N-Type Host for High Efficiency and Long Lifetime in Blue Phosphorescent Organic Light-Emitting Diodes. *ACS Appl. Mater. Interfaces* **2020**, *12*, 19737−19745.

(36) Adachi, C.; Baldo, M. A.; Forrest, S. R.; Thompson, M. E. High-Efficiency Organic Electrophosphorescent Devices with Tris(2-phenylpyridine)Iridium Doped into Electron-Transporting Materials. *Appl. Phys. Lett.* **2000**, *77*, 904.

(37) Li, X. L.; Ye, H.; Chen, D. C.; Liu, K. K.; Xie, G. Z.; Wang, Y. F.; Lo, C. C.; Lien, A.; Peng, J.; Cao, Y.; Su, S. J. Triazole and Pyridine Hybrid Molecules as Electron-Transport Materials for Highly

https://dx.doi.org/10.1021/acsami.0c13705
ACS Appl. Mater. Interfaces 2020, 12, 49895−49904

Efficient Green Phosphorescent Organic Light-Emitting Diodes. *Isr. J. Chem.* **2014**, *54*, 971−978.
(38) Leung, M.-K.; Yang, C.-C.; Lee, J.-H.; Tsai, H.-H.; Lin, C.-F.; Huang, C.-Y.; Su, Y.-O.; Chiu, C.-F. The Unusual Electrochemical and Photophysical Behavior of 2,2'-Bis(1,3,4-oxadiazol-2-yl)biphenyls, Effective Electron Transport Hosts for Phosphorescent Organic Light Emitting Diodes. *Org. Lett.* **2007**, *9*, 235−238.
(39) So, F., Eds. *Organic Electronics-Materials, Processing, Devices and Applications*; CRC Press: Taylor & Francis Group, Boca Raton, FL, 2010.
(40) Tsutsui, T.; Yamamato, K. Evaluation of True Power Luminous Efficiency from Experimental Luminance Values. *Jpn. J. Appl. Phys.* **1999**, *38*, 2799−2803.
(41) Becke, A. D. Density-Functional Exchange-Energy Approximation with Correct Asymptotic Behavior. *Phys. Rev. A* **1988**, *38*, 3098−3100.
(42) Frisch, M. J.; Trucks, G. W.; Schlegel, H. B.; Scuseria, G. E.; Robb, M. A.; Cheeseman, J. R.; Scalmani, G.; Barone, V.; Mennucci, B.; Petersson, G. A.; Nakatsuji, H.; Caricato, M.; Li, X.; Hratchian, H. P.; Izmaylov, A. F.; Bloino, J.; Zheng, G.; Sonnenberg, J. L.; Hada, M.; Ehara, M.; Toyota, K.; Fukuda, R.; Hasegawa, J.; Ishida, M.; Nakajima, T.; Honda, Y.; Kitao, O.; Nakai, H.; Vreven, T.; Montgomery, J. A., Jr.; Peralta, J. E.; Ogliaro, F.; Bearpark, M.; Heyd, J. J.; Brothers, E.; Kudin, K. N.; Staroverov, V. N.; Kobayashi, R.; Normand, J.; Raghavachari, K.; Rendell, A.; Burant, J. C.; Iyengar, S. S.; Tomasi, J.; Cossi, M.; Rega, N.; Millam, J. M.; Klene, M.; Knox, J. E.; Cross, J. B.; Bakken, V.; Adamo, C.; Jaramillo, J.; Gomperts, R.; Stratmann, R. E.; Yazyev, O.; Austin, A. J.; Cammi, R.; Pomelli, C.; Ochterski, J. W.; Martin, R. L.; Morokuma, K.; Zakrzewski, V. G.; Voth, G. A.; Salvador, P.; Dannenberg, J. J.; Dapprich, S.; Daniels, A. D.; Farkas, Ö.; Foresman, J. B.; Ortiz, J. V.; Cioslowski, J.; Fox, D. J. *Gaussian 09*, Revision A.02, Gaussian Inc.: Wallingford CT, 2016.
(43) Zhang, Y.; Wang, K.; Zhuang, G.; Xie, Z.; Zhang, C.; Cao, F.; Pan, G.; Chen, H.; Zou, B.; Ma, Y. Multicolored-Fluorescence Switching of ICT-Type Organic Solids with Clear Color Difference: Mechanically Controlled Excited State. *Chem. − Eur. J.* **2015**, *21*, 2474−2479.
(44) Li, S. W.; Yu, C. H.; Ko, C. L.; Chatterjee, T.; Hung, W. Y.; Wong, K. T. Cyanopyrimidine-Carbazole Hybrid Host Materials for High Efficiency and Low-Efficiency Roll-Off TADF OLEDs. *ACS Appl. Mater. Interfaces* **2018**, *10*, 12930−12936.
(45) Hung, W. Y.; Tu, G. M.; Chen, S. W.; Chi, Y. Phenylcarbazole-Dipyridyl Triazole Hybrid as Bipolar Host Material for Phosphorescent OLEDs. *J. Mater. Chem.* **2012**, *22*, 5410−5418.
(46) Murawski, C.; Leo, K.; Gather, M. C. Efficiency Roll-Off in Organic Light-Emitting Diodes. *Adv. Mater.* **2013**, *25*, 6801−6827.
(47) Ying, S.; Yang, D.; Qiao, X.; Dai, Y.; Sun, Q.; Chen, J.; Ahamad, T.; Alshehri, S. M.; Ma, D. Improvement of Efficiency and Its Roll-off at High Brightness in White Organic Light-Emitting Diodes by Strategically Managing Triplet Excitons in the Emission Layer. *J. Mater. Chem. C* **2018**, *6*, 10793−10803.

https://dx.doi.org/10.1021/acsami.0c13705
ACS Appl. Mater. Interfaces 2020, 12, 49895−49904